Nanoscale Research Letters

NANO EXPRESS

Open Access

ZrO_x Negative Capacitance Field-Effect Transistor with Sub-60 Subthreshold Swing Behavior

Siqing Zhang[†], Huan Liu[†], Jiuren Zhou, Yan Liu[*], Genquan Han and Yue Hao

Abstract

Here we report the ZrO_x-based negative capacitance (NC) FETs with 45.06 mV/decade subthreshold swing (SS) under ± 1 V V_{GS} range, which can achieve new opportunities in future voltage-scalable NCFET applications. The ferroelectric-like behavior of the Ge/ZrO_x/TaN capacitors is proposed to be originated from the oxygen vacancy dipoles. The NC effect of the amorphous HfO_2 and ZrO_x films devices can be proved by the sudden drop of gate leakage, the negative differential resistance (NDR) phenomenon, the enhancement of *I*DS and sub-60 subthreshold swing. 5 nm ZrO_x-based NCFETs achieve a clockwise hysteresis of 0.24 V, lower than 60 mV/decade SS and an 12% *I*DS enhancement compared to the control device without ZrO_x. The suppressed NC effect of Al_2O_3/HfO_2 NCFET compared with ZrO_x NCFET is related to the partial switching of oxygen vacancy dipoles in the forward sweeping due to negative interfacial dipoles at the Al_2O_3/HfO_2 interface.

Keywords: Amorphous ZrO_x, Ferroelectric, FET, Subthreshold swing, Negative capacitance

Background

As complementary metal oxide semiconductor (CMOS) devices scaling down constantly, the integrated circuit (IC) technique has entered into the era of "more than Moore era". The driving force of IC industry and technology becomes the reduction of power consumption, instead of the miniaturization of transistors [1, 2]. However, the Boltzmann tyranny of MOSFETs, more than 60 mV/decade SS has restricted the energy/power efficiency [3]. In recent years, many proposed novel devices have the ability to achieve sub-60 mV/decade threshold swing, including impact ionization MOSFETs, tunnel FETs and NCFETs [4–7]. Due to the simple structure, the steep SS and improved drive current, NCFETs with a ferroelectric (FE) film have been regarded as an attractive alternative among these emerging devices [8–10]. The reported experiments on NCFETs mainly include $PbZrTiO_3$ (PZT), P(VDF-TrFE) and $HfZrO_x$ (HZO) [11–17]. However, the high process temperature and undesired gate leakage current along the grain boundaries of polycrystalline ferroelectric materials have restricted their development for the state-of-the-art technology nodes [18–26]. Recently, ferroelectricity in the amorphous Al_2O_3 and ZrO_x films enabled by the voltage-modulated oxygen vacancy dipoles has been investigated [27–29]. Compared with the crystalline counterpart, the amorphous ferroelectric-like films have significant advantages in reduced process temperature and leakage current. Thus, there are mass researches on FeFETs with amorphous gate insulator for the non-volatile memory and analog synapse applications [27, 30–34]. However, the systematical investigation on one-transistor ZrO_x-based NCFET has not been carried out.

In this work, Ge NCFETs with 5 nm ZrO_x ferroelectric dielectric layer and 5 nm Al_2O_3/HfO_2 ferroelectric dielectric layer have been proposed, respectively. We experimentally observed sub-60 mV/decade steep slope in ZrO_x (5 nm) NCFET, which can be attributed to the

*Correspondence: xdliuyan@xidian.edu.cn
[†]Siqing Zhang and Huan Liu have contribute equally to this work
State Key Discipline Laboratory of Wide Band Gap Semiconductor Technology, School of Microelectronics, Xidian University, Xi'an 710071, China

NC effect of ZrO_x ferroelectric layer. And we analyzed the polarization *P* as function of applied voltage *V* for the $Ge/ZrO_x/TaN$ capacitors. The ferroelectric-like behavior of the $Ge/ZrO_x/TaN$ capacitors is induced by the voltage-induced oxygen vacancy dipoles. Moreover, we attributed the improved I_{DS} and the sudden drop of I_G in the Al_2O_3/HfO_2 NCFETs and ZrO_x NCFETs to the NC effect. We also observed the NDR phenomenon in the Al_2O_3/HfO_2 NCFETs and ZrO_x NCFETs. In addition, we further analyzed the physical mechanism of interfacial dipoles-induced decreased NC effect in the Al_2O_3/HfO_2 NCFET. The ZrO_x NCFETs with sub-60 mV/decade steep slope, improved drain voltage and low operating voltage will be suit for the design of NCFETs with low power consumption in the "more than Moore era".

Methods

Key process steps for NCFETs with ZrO_x and Al_2O_3/HfO_2 fabrication are shown in Fig. 1a. Different gate dielectric insulators, including Al_2O_3/amorphous HfO_2 (5 nm) films and amorphous ZrO_x (4.2 nm) films were grown on n-Ge (001) substrates by atomic layer deposition (ALD) at 300 °C. TMA, TDMAHf, TDMAZr and H_2O vapor were used as the precursors of Al, Hf, Zr and O, respectively. The pulse time and purge time of the precursors of Hf and Zr are 1.6 s and 8 s, respectively. The pulse time and purge time of the precursors of Al are 0.2 s and 8 s, respectively. A TaN top gate electrode was then deposited on HfO_2 or ZrO_x surfaces by reactive sputtering. Source/drain (S/D) regions were defined by lithography patterning and dry etching. After that, boron (B^+) and nickel (Ni) was deposited in source/drain (S/D) regions. Finally, rapid thermal annealing (RTA) at 350 °C for 30 s in a 10^8 Pa nitrogen ambient was carried out. Figure 1b, d show the schematics of the fabricated Al_2O_3/HfO_2 NCFETs and ZrO_x NCFETs. High-resolution transmission electron microscope (HRTEM) image in Fig. 1c depicts the amorphous HfO_2 (5 nm) film on Ge (001) with Al_2O_3 interfacial layer. HRTEM image in Fig. 1e depicts the amorphous ZrO_x (4.2 nm) film on Ge (001). The C–V curve of ZrO_x NCFETs and the X-ray photoelectron spectra (XPS) of TaN/ZrO_x (4.2 nm)/Ge capacitors were measured in Additional file 1: Fig. S1.

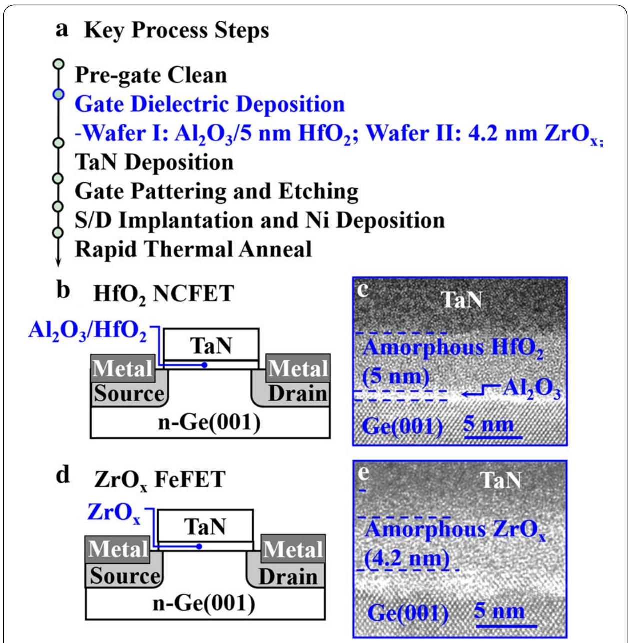

Fig. 1 **a** Key process steps for the fabrication of the Al_2O_3/5 nm HfO_2 NCFETs and 4.2 nm ZrO_x NCFETs. **b** Schematics and **c** HRTEM images of the fabricated ZrO_x NCFETs. **d** Schematics and **e** HRTEM images of the fabricated Al_2O_3/HfO_2 NCFETs

Results and Discussion

Figure 2a shows the measured curves of polarization *P v.s.* applied voltage *V* characteristics for the $Ge/ZrO_x/TaN$ capacitors at 3.3 kHz. The gate length (L_G) of the capacitors are 8 μm. It is observed that the remnant polarization P_r of the $Ge/ZrO_x/TaN$ capacitors can be enhanced with larger sweeping range of *V*. The ferroelectric-like behavior of the amorphous ZrO_x film in the Fig. 2a is proposed to be originated from the voltage-driven oxygen vacancy dipoles [35]. Figure 2b shows the measured *P*–*V* curves for the $Ge/ZrO_x/TaN$ capacitors under different frequencies from 200 to 10 kHz. We can see that the ferroelectric-like behavior of the amorphous ZrO_x film remain stable for all frequencies. However, the P_r of the amorphous ZrO_x film is reduced with the increased frequencies. This phenomenon can be explained by the incomplete dipoles switching under high measurement frequencies [36, 37]. As measurement frequencies

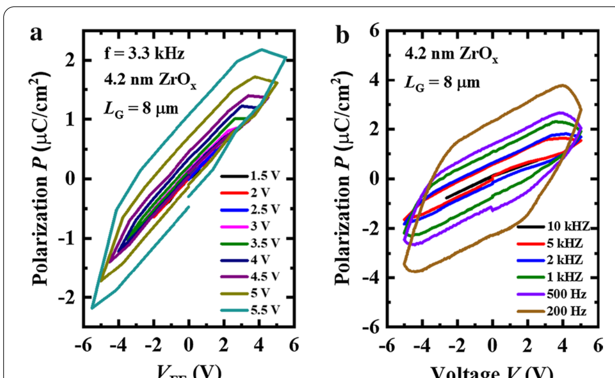

Fig. 2 Measured *P* versus *V* characteristics of the 4.2 nm ZrO_x capacitors with **a** different sweeping ranges of *V* and **b** different measurement frequences

increasing, the time for the direction change of electric field in the amorphous ZrO_x film decreases. Thus, part of oxygen vacancy diploes switching is incomplete, providing decreased P_r.

Figure 3a shows the measured I_{DS}–V_{GS} curves of a ferroelectric Al_2O_3/HfO_2 NCFET at the V_{DS} of −0.05 V and −0.5 V. The L_G of the devices is 3 μm. The hysteresis loops of 0.14 V ($V_{DS} = -0.05$ V, $I_{ds} = 1$ nA/μm) and 0.08 V ($V_{DS} = -0.5$ V, $I_{ds} = 1$ nA/μm) are demonstrated, respectively. The clockwise hysteresis loops are attributed to the migration of oxygen vacancies and accompanied negative charges. The oxygen vacancy dipoles accumulate (deplete) in the Ge/Al_2O_3 interface under positive (negative) V_{GS}. Therefore, the threshold voltage (V_{TH}) increases (decreases) under forward (reverse) sweeping of gate voltages. As shown in Fig. 3b, the output characteristics of the Al_2O_3/HfO_2 NCFET and the control FET are compared. The saturation current of the Al_2O_3/HfO_2 NCFET exceeds 26 μA/μm, with a rise of 23% compared to that of the control FET at $|V_{GS}–V_{TH}| = |V_{DS}| = 0.8$ V. The current enhancement is induced by the increased inversion charge intensity (Q_{inv}) in the reverse polarization electric field and the amplification of surface potential [38, 39]. In addition to current enhancement, the obtained obvious NDR proves the NC effect of the amorphous HfO_2 film. The NDR effect is caused by the incomplete switching of oxygen vacancy dipoles due to the coupling of drain-to-channel as V_{DS} increases [40, 41]. Figure 3c compares the measured gate leakage I_G–V_{GS} curves for the 5 nm Al_2O_3/HfO_2 NCFET at the V_{DS} of −0.05 V and −0.5 V. The sudden drops of I_G only during the reverse sweeping indicate the decreased voltage in the amorphous HfO_2 film and the amplication of surface potential [42]. The absence of NC effect during the forward sweeping is caused by the partical switching of oxygen vacancy dipoles in the amorphous HfO_2 film [43]. The different ability to contain oxygen atoms between Al_2O_3 and HfO_2 layer leads to oxygen redistribution and negative interfacial dipoles at the Al_2O_3/HfO_2 interface [44, 45]. Due to the presence of negative interfacial dipoles, it is difficult for the amorphous HfO_2 film to realize complete polarization switching (NC effect) in the forward sweeping (Additional file 1).

Figure 4a shows the measured transfer curves of a ferroelectric ZrO_x NCFET at the V_{DS} of −0.05 V and −0.5 V. The L_G of the two devices are 4 μm. The clockwise hysteresis loops of 0.24 V ($V_{DS} = -0.05$ V, $I_{ds} = 1$ nA/μm) and 0.14 V ($V_{DS} = -0.5$ V, $I_{DS} = 1$ nA/μm) are demonstrated, respectively. As shown in Fig. 4b, the output characteristics of the ZrO_x NCFET and the control FET are compared. The saturation current of the ZrO_x NCFET exceeds 30 μA/μm, with a rise of 12% compared to that of the control FET at $|V_{GS}–V_{TH}| = |V_{DS}| = 1$ V. The improved current enhancement and more obvious NDR indicate the enhanced NC effect of the amorphous ZrO_x film (5 nm) contrast to that of 5 nm HfO_2 film. Figure 4c compares the measured gate leakage I_G–V_{GS} curves for the 5 nm ZrO_x NCFET at the V_{DS} of −0.05 V and −0.5 V. Compared to the sudden I_G drops of Al_2O_3/HfO_2 NCFET only during reverse sweeping in Fig. 3c, the sudden drops of I_G both in forward and reverse sweeping in Fig. 4c also prove the enhanced NC effect in the amorphous ZrO_x film.

Figure 5a, b shows the point SS as function of I_{DS} for the Al_2O_3/HfO_2 and ZrO_x NCFET at the V_{DS} of −0.05 V and −0.5 V. As shown in Fig. 5b, sub-60 mV/decade subthreshold swing (SS) can be achieved during forward or reverse sweeping of V_{GS} at the V_{DS} of −0.05 V and −0.5 V. When V_{DS} is −0.05 V, a point forward SS of 45.1 mV/dec and a point reverse SS of 55.2 mV/dec were achieved. When V_{DS} is −0.5 V, a point forward SS of 51.16 mV/dec and a point reverse SS of 46.52 mV/dec were achieved.

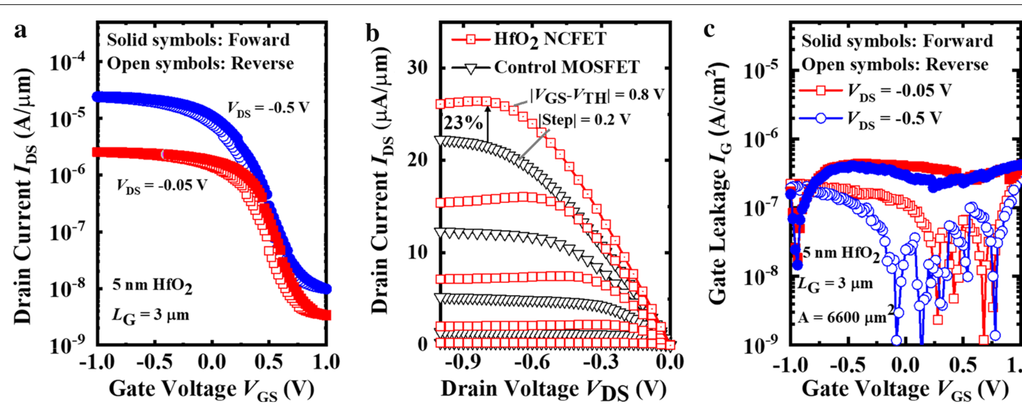

Fig. 3 **a** Measured I_{DS}–V_{GS} curves of the 5 nm HfO_2 NCFET when $V_{DS} = -0.5$ V and $V_{DS} = -0.05$ V. **b** Measured I_{DS}–V_{DS} curves of the HfO_2 NCFET and the control MOSFET. **c** Measured I_G–V_{GS} curves of the 5 nm HfO_2 NCFET when $V_{DS} = -0.5$ V and $V_{DS} = -0.05$ V

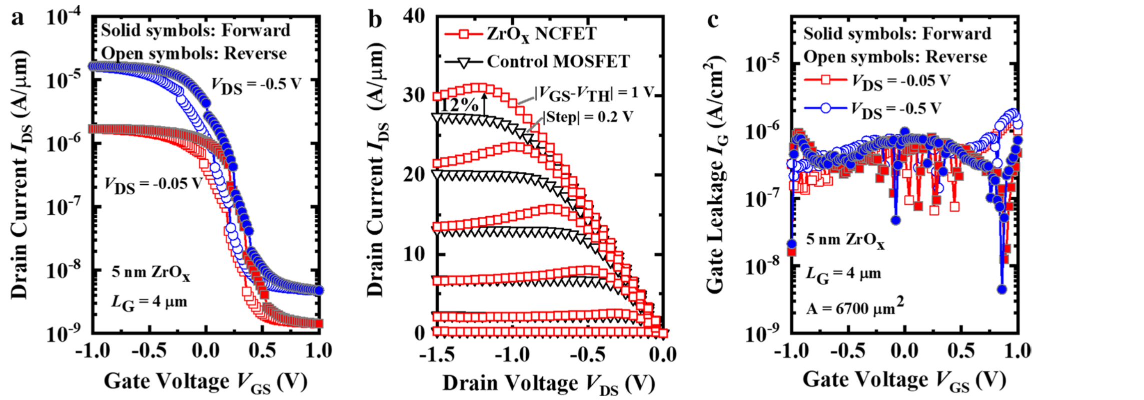

Fig. 4 **a** Measured I_{DS}–V_{GS} curves of the 5 nm ZrO_x NCFET when $V_{DS} = -0.5$ V and $V_{DS} = -0.05$ V. **b** Measured I_{DS}–V_{DS} curves of the ZrO_x NCFET and the control MOSFET demonstraing the obvious NDR phenomenon. **c** Measured I_G–V_{GS} curves of the 5 nm ZrO_x NCFET when $V_{DS} = -0.5$ V and $V_{DS} = -0.05$ V

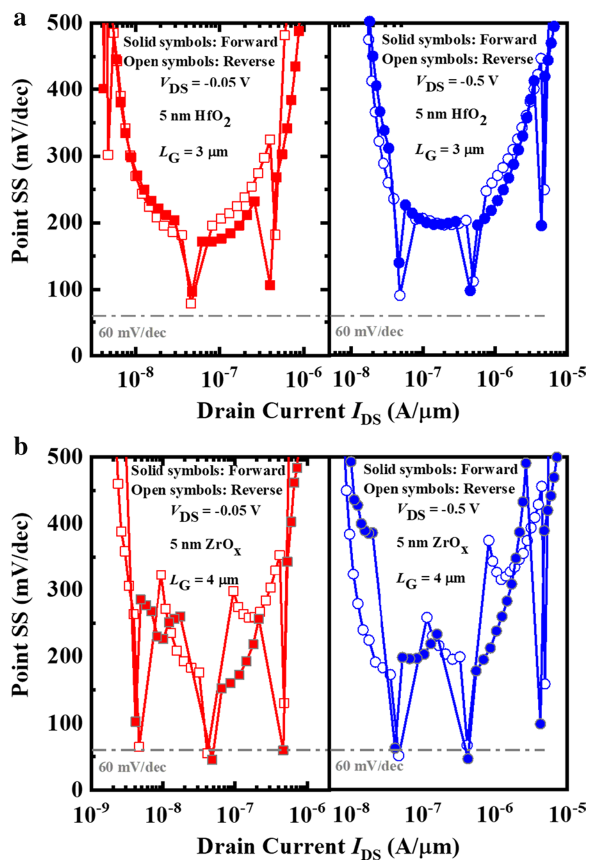

Fig. 5 Point SS as a function of I_{DS} for the **a** Al_2O_3/5 nm HfO_2 NCFETs and **b** 5 nm ZrO_x NCFETs

Due to the different ability of scavenging effect for the Al_2O_3/HfO_2 and ZrO_x layer, the partical dipoles switching is caused in the Al_2O_3/HfO_2 NCFET. Therefore, the more obvious NC effect with sub-60 mV/decade SS is achieved in 5 nm ZrO_x NCFET.

Conclusions

We report the demonstration of ferroelectric NC ZrO_x pFETs with the sub-60 mV/decade SS, low operating voltage of 1 V and a hysteresis of less than 60 mV. The impact of the amorphous ZrO_x films on the ferroelectric behavior is explained by the oxygen vacancy dipoles. The improved I_{DS} and NDR phenomenon are also obtained in Al_2O_3/HfO_2 NCFETs and ZrO_x NCFETs compared to the control device. The suppressed NC effect of the Al_2O_3/HfO_2 NCFET can be attributed to partical dipole swiching due to interfical dipoles at the Al_2O_3/HfO_2 interface. The ZrO_x NCFETs with sub-60 mV/decade steep slope, improved drain voltage and low operating voltage pave a new way for future low power consumption NCFETs design.

Supplementary Information

The online version contains supplementary material available at https://doi.org/10.1186/s11671-020-03468-w.

Additional file 1. From the C–V curve of ZrO_x NCFETs in Fig. S1 (a), we can see that the threshold voltage of the ZrO_x NCFETs is around 0.5 V. From the XPS of TaN/ZrO_x (4.2 nm)/Ge capacitors in Fig. S1 (b), we can see that a TaO_x interfacial layer formed in the TaN/ZrO_x interface and oxygen vacancies (ZrO_x) in ZrO_x because of the scavenging effect.

Abbreviations

TaN: Tantalum nitride; ZrO_x: Zirconium dioxide; TDMAZr: Tetrakis (dimethylamido) zirconium; P_r: Remnant polarization; E_c: Coercive electric field; MOSFETs: Metal–oxide–semiconductor field-effect transistors; Ge: Germanium; ALD: Atomic layer deposition; B^+: Boron ion; Al_2O_3: Aluminum oxide; HRTEM: High-resolution transmission electron microscope; Ni: Nickel; RTA: Repaid thermal annealing; I_{DS}: Drain current; V_{GS}: Gate voltage; V_{TH}: Threshold voltage; NCFET: Negative capacitance field-effect transistor.

Acknowledgements
Not applicable.

Authors' Contributions
SQZ and HL drafted the manuscript and carried out the experiments. YL designed the experiments. YL and JRZ helped to revise the manuscript. YH and GQH supported the study. All the authors read and approved the final manuscript.

Funding
The authors acknowledge support from the National Key Research and Development Project (Grant No. 2018YFB2202800, 2018YFB2200500) and the National Natural Science Foundation of China (Grant No. 62025402, 62090033, 91964202, 92064003, 61874081, 61851406, 62004149 and 62004145).

Availability of Data and Materials
The datasets supporting the conclusions of this article are included in the article.

Competing interests
The authors declare that they have no competing interests.

Received: 13 September 2020 Accepted: 17 December 2020
Published online: 02 February 2021

References

1. Lundstrom MS. The MOSFET revisited: device physics and modeling at the nanoscale. IEEE Int. SOI Conf. 2006;1–3.
2. Sakurai T. Perspectives of low-power VLSI's. IEICE Trans. Electron. 2004;429–436.
3. Sze SM, Ng KK. Physics of Semiconductor Devices, 3rd Edition. Wiley Inter science; 2006.
4. Baba T (1992) Proposal for surface tunnel transistors. Jpn J Appl Phys 31:4
5. Sarkar D, Xie X, Liu W et al (2015) A subthermionic tunnel field-effect transistor with an atomically thin channel. Nature 526:91–95
6. Gopalakrishnan K, Griffin P, Plummer J (2005) Impact ionization MOS (IMOS)-Part I: device and circuit simulations. IEEE Tran Elec Dev 52:69–76
7. Salahuddin S, Datta S (2008) Use of negative capacitance to provide voltage amplification for low power nanoscale devices. Nano Lett 8:405–410
8. Li KS, Chen PG, Lai TY, et al. Sub-60mV-swing negative-capacitance FinFET without hysteresis. In: IEEE international electron devices meeting. 2016.
9. Khan AI, Yeung CW, Hu C, et al. Ferroelectric negative capacitance MOSFET: capacitance tuning and antiferroelectric operation. IEDM Tech Dig. 2011.
10. Salahuddin S, Datta S (2008) Use of negative capacitance to provide voltage amplification for low power nanoscale devices. Nano Lett 8(2):405–410
11. Dasgupta S, Rajashekhar A, Majumdar K, et al. Sub-kT/q switching in strong inversion in $PbZr_{0.52}Ti_{0.48}O_3$ gated negative capacitance FETs. IEEE J Exploratory Solid-State Comput. Devices Circuits. 2017; 1:43–48.
12. Bakaul S, Serrao C, Lee M et al (2016) Single crystal functional oxides on silicon. Nat Commun 7:10547
13. Rusu A, Salvatore GA, Jimenez D, et al. Metal–ferroelectric–metal–oxide–semiconductor field effect transistor with sub-60 mV/decade subthreshold swing and internal voltage amplification. Electron Devices Meeting. IEDM Tech Dig. 2010.
14. Jo J, Shin C (2016) Negative capacitance field effect transistor with hysteresis-free sub-60-mV/Decade switching. IEEE Electron Device Lett 37:245–248
15. Lee MH, Wei YT, Chu KY et al (2015) Steep slope and near non-hysteresis of FETs with antiferroelectric-like HfZrO for low-power electronics. IEEE Electron Device Lett 36:294–296
16. Cheng CH, Chin A (2014) Low-voltage steep turn-on pMOSFET using ferroelectric high-k gate dielectric. IEEE Electron Device Lett 35:274–276
17. Lee MH, Chen PG, Liu C, et al. Prospects for ferroelectric $HfZrO_x$ FETs with experimentally CET=0.98 nm, SS_{for}=42 mV/dec, SS_{rev}=28 mV/dec, switch-OFF <0.2 V, and hysteresis-free strategies. In: IEEE international electron devices meeting; 2015.
18. Müller J, Yurchuk E, Schlsser T, et al. Ferroelectricity in HfO_2 enables nonvolatile data storage in 28 nm HKMG. In: Symposium on VlSI technology; 2012.
19. Schroeder U, Yurchuk E, Müller J et al (2014) Impact of different dopants on the switching properties of ferroelectric hafnium oxide. Jpn J Appl Phys 53:85–89
20. Mueller S, Muller J, Schroeder U et al (2013) Reliability characteristics of ferroelectric Si:HfO_2 thin films for memory applications. IEEE T Device Mat Re 13:93–97
21. Park MH, Kim HJ, Kim YJ et al (2016) Effect of Zr content on the wake-up effect in $Hf_{1-x}Zr_xO_2$ films. ACS Appl Mater Inter 8:15466–15475
22. Schroeder U, Richter C, Park MH et al (2018) Lanthanum-doped hafnium oxide: a robust ferroelectric material. Inorg Chem 57:2752–2765
23. Chernikova AG, Kozodaev MG, Negrov DV et al (2018) Improved ferroelectric switching endurance of la-doped $Hf_{0.5}Zr_{0.5}$O2 Thin Films. ACS Appl. Mater. Interfaces 10:2701–2708
24. Hyuk PM, Hwan LY, Thomas M et al (2018) Review and perspective on ferroelectric HfO_2-based thin films for memory applications. MRS Commun 8:795–808
25. Mueller S, Yurchuk E, Slesazeck S, et al. Performance investigation and optimization of Si:HfO_2 FeFETs on a 28 nm bulk technology. In: Joint IEEE international symposium on applications of ferroelectric and workshop on piezoresponse force microscopy; 2013;248–51.
26. Zhou J, Zhou Z, Wang X et al (2020) Demonstration of ferroelectricity in Al-doped HfO_2 with a low thermal budget of 500 °C. IEEE Electron Device Lett 41:1130–1133
27. Liu H, Peng Y, Han G et al (2020) ZrO_2 ferroelectric field-effect transistors enabled by the switchable oxygen vacancy dipoles. Nanoscale Res Lett 15:120
28. Peng Y, Han G, Liu F, et al. Non-Volatile Field-Effect Transistors Enabled by Oxygen Vacancy Related Dipoles for Memory and Synapse Applications. IEEE Electron Device Lett. 2020.
29. Peng Y, Han G, Liu F et al (2020) Ferroelectric-like behavior originating from oxygen vacancy dipoles in amorphous film for non-volatile memory. Nanoscale Res Lett 15:134
30. Park MH, Kim HJ, Kim YJ et al (2014) Thin $Hf_xZr_{1-x}O_2$ films: a new lead-free system for electrostatic supercapacitors with large energy storage density and robust thermal stability. Adv Energy Mater 4:1400610
31. Schroeder U, Yurchuk E, Mueller J et al (2014) Impact of different dopants on the switching properties of ferroelectric hafnium oxide. Jpn J Appl Phys 53:08LE02
32. Peng Y, Xiao W, Liu F et al (2020) Non-volatile field-effect transistors enabled by oxygen vacancy related dipoles for memory and synapse applications. IEEE Electron Device Lett 67:3632–3636
33. Peng Y, Han G, Liu F et al (2020) Ferroelectric-like behavior originating from oxygen vacancy dipoles in amorphous film for non-volatile memory. Nanoscale Res Lett 5:134
34. Zhang S, Liu Y, Zhou J et al (2020) Low voltage operating 2D MoS_2 ferroelectric memory transistor with $Hf_{1-x}Zr_xO_2$ gate structure. Nanoscale Res Lett 15:157
35. Glinchuk MD, Morozovska AN, Lukowiak A et al (2020) Possible electrochemical origin of ferroelectricity in HfO_2 thin films. J Alloy Compod 830:153628
36. Ishibashi Y, Orihara H (1995) A theory of D–E hysteresis loop. Integr Ferroelectr 9:57–61
37. Scott JF, Dawber M (2000) Atomic-scale and nanoscale self-patterning in ferroelectric thin films. AIP Conf Proc 535:129
38. Chen HP, Lee VC, Ohoka A et al (2011) Modeling and design of ferroelectric MOSFETs. IEEE Trans Electron Devices 58:2401–2405
39. Zhou J, Peng Y, Han G et al (2017) Hysteresis reduction in negative capacitance ge pfets enabled by modulating ferroelectric properties in $HfZrO_x$. IEEE J Electron Dev 6:41–48
40. Saha AK, Sharma P, Dabo I, et al. Ferroelectric transistor model based on self-consistent solution of 2D Poisson's, non-equilibrium Green's

function and multi-domain Landau Khalatnikov equations. In: IEEE international electron devices meeting. 2018.
41. Zhou J, Han G, Li J et al (2018) Negative differential resistance in negative capacitance FETs. IEEE Electron Device Lett 39:622–625
42. Zhou J, Han G, Li Q, et al. Ferroelectric $HfZrO_x$ Ge and GeSn PMOSFETs with Sub-60 mV/decade subthreshold swing, negligible hysteresis, and improved I_{ds}. In: IEEE international electron devices meeting. 2017.
43. Sharma P, Tapily K, Saha AK, et al. Impact of total and partial dipole switching on the switching slope of gate-last negative capacitance FETs with ferroelectric hafnium zirconium oxide gate stack. In: Symposium on VLSI technology. 2017.
44. Lin L, Robertson J (2011) Atomic mechanism of electric dipole formed at high-K: SiO_2 interface. J Appl Phys 109:9
45. Sharia O, Demkov AA, Bersuker G et al (2007) Theoretical study of the insulator/insulator interface: band alignment at the SiO_2/HfO_2 junction. Phys Rev B 75:3

Publisher's Note